Yaguo Wang

Bo Qiu

School of Mechanical Engineering
and Birck Nanotechnology Center,
Purdue University,
West Lafayette, IN 47907

Alan J. H. McGaughey
Department of Mechanical Engineering,
Carnegie Mellon University,
Pittsburgh, PA 15213

Xiulin Ruan

Xianfan Xu
e-mail: xxu@ecn.purdue.edu

School of Mechanical Engineering
and Birck Nanotechnology Center,
Purdue University,
West Lafayette, IN 47907

Mode-Wise Thermal Conductivity of Bismuth Telluride

Thermal properties and transport control are important for many applications, for example, low thermal conductivity is desirable for thermoelectrics. Knowledge of mode-wise phonon properties is crucial to identify dominant phonon modes for thermal transport and to design effective phonon barriers for thermal transport control. In this paper, we adopt time-domain (TD) and frequency-domain (FD) normal-mode analyses to investigate mode-wise phonon properties and to calculate phonon dispersion relations and phonon relaxation times in bismuth telluride. Our simulation results agree with the previously reported data obtained from ultrafast time-resolved measurements. By combining frequency-dependent anharmonic phonon group velocities and lifetimes, mode-wise thermal conductivities are predicted to reveal the contributions of heat carriers with different wavelengths and polarizations. [DOI: 10.1115/1.4024356]

Keywords: phonon dispersion, phonon lifetime, bismuth telluride, thermal conductivity

1 Introduction

Lattice thermal conductivity is associated with phonon transport [1]. For many applications, thermal transport properties and thermal transport control are important, for example, low thermal conductivity is desirable for thermoelectrics. To tailor lattice thermal conductivity effectively, a detailed understanding of mode-wise phonon properties is necessary. Because of limitations of experimental techniques, which only detect several specific phonon modes, numerical approaches are needed to obtain a complete picture of phonon dynamics [2]. As such, dominant phonon modes for thermal transport can be identified and various phonon barriers can be designed to tailor thermal transport properties [3].

For bismuth telluride (Bi_2Te_3), a widely used thermoelectric material, phonon dynamics of a number of phonon modes has been studied in experiments using ultrafast time-resolved techniques [4–6]. Although molecular dynamics (MD) simulations have been performed to predict lattice thermal conductivity [7,8], no detailed theoretical work has been performed to reveal mode-wise phonon relaxation times and mode-wise thermal conductivity in bismuth telluride.

In this study, we adopt two-body interatomic potentials to study the anharmonic mode-wise phonon properties of bulk Bi_2Te_3 using TD and FD normal-mode analysis (NMA). The predicted phonon velocities and phonon life times at a number of modes in Bi_2Te_3 are compared with experimental results. Our calculations also yield mode-wise lattice thermal conductivity, which is helpful for analyzing thermal transport in nanostructured materials.

2 Numerical Methods

MD is a powerful tool for studying details of phonon dynamics. A requirement for MD studies is a suitable potential function that describes interatomic interactions. Bulk Bi_2Te_3 has a rhombohedral primitive cell belonging to the space group $R\bar{3}m$. At room temperature, the corresponding conventional cell is hexagonal, consisting of periodic fivefold layer along the c-axis: Te_1–Bi–Te_2–Bi–Te_1. The bonding force is covalent within the fivefold layer and van der Waals between the layers [7]. The nearest-neighbor distances between atoms in different monatomic layers are 3.04 Å for Te_1–Bi bond, 3.24 Å for Te_2–Bi bond, and 3.72 Å for Te_1–Te_1 bond [9]. Huang and Kaviany developed a set of three-body potentials for bulk Bi_2Te_3 [7]. Even though the properties predicted by this 24-parameter-potential agree well with experimental results, the computation cost is prohibitive to implement it into MD simulations. Qiu and Ruan developed two-body potentials using density-functional theory calculations [8], which we use here. The lattice thermal conductivities predicted from this potential agree with experimental results between temperatures of 150 to 500 K [8]. The two-body potentials are expressed as follows:

$$U_{ij} = U_{ij}^{s} + \frac{q_i q_j}{r_{ij}} = D_e\left\{[1 - \exp[-\sigma(r_{ij} - r^0)]]^2\right\} + \frac{q_i q_j}{r_{ij}} \quad (1)$$

Here, the short-range potential U_{ij}^{s} takes the Morse form, where D_e corresponds to the depth of potential well, r^0 denotes the equilibrium bond distance, and σ is the bond elasticity. The parameters for the short-range potentials are listed in Table 1. Only the nearest-neighbor interactions are considered in this set of potentials and r_c represents the cut-off distance for each pair of atoms. To evaluate the long-range Coulomb interaction effectively, Wolf's summation [10] was applied with a cut-off radius of 11.28 Å. q_i and q_j the last terms in Eq. (1) are the effective charges of the ions, which are 0.38, −0.26, and −0.24 for Bi, Te_1, and Te_2, respectively [8].

The lattice thermal conductivity κ_L is the sum over the contributions from all phonon modes in the first Brillouin zone, κ_j for mode j, called mode-wise thermal conductivity [11]

$$\kappa_L = \sum_j \kappa_j = \sum_\alpha \int C_V v_g^2 \tau d\vec{k} \quad (2)$$

Contributed by the Heat Transfer Division of ASME for publication in the Journal of Heat Transfer. Manuscript received June 10, 2012; final manuscript received November 2, 2012; published online July 26, 2013. Assoc. Editor: Pamela M. Norris.

Table 1 Parameters of short-range potential [8]

Bond	D_e (eV)	σ (1/Å)	r^0 (Å)	r_c (Å)
Bi–Bi	0.085	2.212	4.203	5.5
Bi–Te_1	0.975	1.285	3.089	4.0
Bi–Te_2	0.582	1.257	3.251	4.0
Te_1–Te_1	0.076	1.675	3.642	5.0
Te_1–Te_2	0.807	0.731	4.497	5.5
Te_2–Te_2	0.066	2.876	4.312	5.0

where α corresponds to the mode polarization (LA, TA, LO, and TO). As shown in Eq. (2), the three components of κ_j include mode-wise volumetric heat capacity C_V, phonon velocity v_g, and phonon lifetime τ. Since Bi_2Te_3 has a relatively low Debye temperature, 155 K, we can simply use the high temperature limit $C_V = k_B/V$ to estimate thermal conductivity at 300 K, where k_B is the Boltzmann constant where V is the volume of the MD simulation cell. The second component anharmonic phonon velocity is the gradient of anharmonic phonon dispersion, $v = \partial\omega/\partial k$, where $\vec{k}$ is the phonon wave vector and ω is the phonon angular frequency. The third component is the anharmonic phonon lifetime. Hence, in determining the mode-wise thermal conductivity κ_j, two key quantities need to be calculated: the anharmonic phonon dispersion and the phonon lifetime. In what follows, two numerical approaches—TD-NMA and FD-NMA will be described for predicting the anharmonic phonon dispersion and the phonon lifetime in bulk Bi_2Te_3.

2.1 TD-NMA for Computing Anharmonic Phonon Dispersion and Phonon Lifetimes. The time-domain normal-mode analysis is based on lattice dynamics (LD). The essential part of LD is to solve the equations of motion of the lattice which is represented in the form of a dynamical matrix. The eigenvectors of the dynamical matrix are the polarization vectors of atomic motions and the square roots of corresponding eigenvalues are phonon frequencies. The wave-like solutions of LD represent uncoupled motions of orthogonal oscillators, called normal modes. Any harmonic motion can be exactly expressed as a superposition of normal modes. Harmonic displacement of individual atoms can be written as the summation of all of the normal modes [12]

$$\hat{d}_i(t) = N^{1/2} \sum_{\vec{k},\alpha} S(\alpha,\vec{k})\vec{\varepsilon}(\alpha,\vec{k}) \exp\left[i(\vec{k}\cdot\vec{r}_i^{\,0} - \omega(\alpha,\vec{k})t)\right] \tag{3}$$

where S denotes the normal-mode amplitude and $\vec{\varepsilon}$ is the polarization vector associated with the direction of motions. $\vec{r}_i^{\,0}$ is the equilibrium position of each atom denoted by i. Conversely, the amplitude of every normal mode can be written as the summation of displacements of all atoms

$$S_j(\alpha,\vec{k}) = N^{-1/2} \sum_i m_i^{\frac{1}{2}} \exp(-i\vec{k}\cdot\vec{r}_i^{\,0})\vec{\varepsilon}_j^{\,*}(\alpha,\vec{k})\cdot\hat{d}_i \tag{4}$$

where * denotes the complex conjugate. The harmonic angular frequency ω and polarization vector $\vec{\varepsilon}$ are computed through diagonalizing the dynamical matrix in LD using the software GULP [13]. $\vec{k}$ is specified based on the crystal structure and the size of the MD domain. m is the atomic mass, 208.98 for Bi and 127.60 for Te. $\hat{d}_i = \vec{r}_i - \vec{r}_i^{\,0}$ represents the displacement of atom i from its equilibrium position $\vec{r}_i^{\,0}$. The equilibrium position $\vec{r}_i^{\,0}$ and displacement $\hat{d}_i$ are computed from MD using the potential function described in Eq. (1).

The total energy of an individual mode under harmonic approximation is computed as

$$E_j(t) = E_{j,P} + E_{j,K} = \frac{\omega_j^2 \hat{S}_j^* \hat{S}_j}{2} + \frac{\dot{\hat{S}}_j^* \dot{\hat{S}}_j}{2} \tag{5}$$

where $E_{j,P}$ is the potential energy, $E_{j,K}$ is the kinetic energy, ω_j is the quasi-harmonic angular frequency, and "·" indicates derivative. The anharmonic phonon frequency is half of the oscillating frequency of autocorrelation function of mode-wise potential energy or kinetic energy [14]. Therefore, for every specified wave vector, the corresponding anharmonic phonon frequency at finite temperatures can be extracted from the oscillations of autocorrelation of mode-wise potential/kinetic energy obtained from Eq. (5). Applying this to all of the sampled wave vectors in the first Brillouin zone, anharmonic phonon dispersion curves can be constructed.

A number of studies have investigated phonon lifetimes. The decay of the autocorrelation of the total energy of argon was used to deduce the effective phonon lifetimes [15]. Henry and Chen [2] employed the definition of Ladd et al. [16] to extract phonon lifetime of silicon. For bismuth telluride, it is not trivial to perform exponential fitting of the autocorrelation of the total energy due to residual oscillation. Also, the phonon lifetimes defined by Ladd et al. are not easy to converge because the numerical errors overwhelm the actual phonon signal at longer time. Therefore, as depicted in Fig. 1, we obtain the phonon relaxation time via fitting a time constant of the integrated autocorrelation of potential energy.

Figure 1 also shows the oscillations of the autocorrelation function of mode-wise potential energy, which has a frequency twice of the corresponding anharmonic phonon frequency. In a sense, NMA bridges the real space analysis and the phonon space analysis by mapping the anharmonic information obtained in MD (atomic displacement) to the phonon space with normal-mode amplitude S.

2.2 FD-NMA. An alternative approach is the frequency-domain normal-mode analysis. According to Ladd et al. [16], the normal-mode amplitude can be written under the single mode relaxation time approximation as

$$S_j(\alpha,\vec{k}) = S_{j,0}(\alpha,\vec{k})e^{-i(\omega(\alpha,\vec{k})-i\Gamma(\alpha,\vec{k}))t} \tag{6}$$

where the phonon spectral linewidth Γ is related to phonon lifetime τ as follows:

$$\tau = 1/2\Gamma \tag{7}$$

Then, the Fourier transform of the time derivative of normal-mode amplitude as given in Eq. (6) is

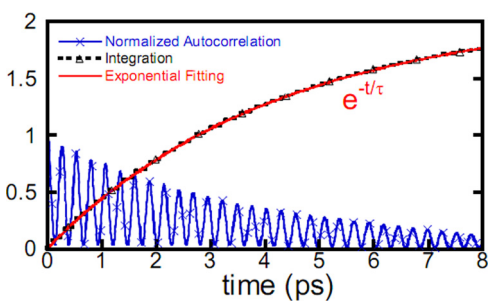

Fig. 1 Normalized autocorrelation of phonon potential energy, integration of the autocorrelation, and the exponential fitting to deduce phonon relaxation time

$$F[\dot{S}_j(\alpha,\vec{k})] = \frac{1}{\sqrt{2\pi}}\int_{-\infty}^{\infty} S_{j,0}(\alpha,\vec{k})(-i\omega(\alpha,\vec{k}) - \Gamma(\alpha,\vec{k})) \times e^{-i(\omega(\alpha,\vec{k})-\omega)t} e^{-\Gamma(\alpha,\vec{k})t} dt \quad (8)$$

If we define the spectral energy density (SED) function as the norm square of Eq. (8), then it can be shown that the SED function is in the Lorentzian form [17]

$$\psi(\alpha,\vec{k},f) \equiv \left|F[\dot{S}_j(\alpha,\vec{k})]\right|^2 = \frac{C(\alpha,\vec{k})}{[4\pi\tau(\alpha,\vec{k})(f - f(\alpha,\vec{k})]^2 + 1} \quad (9)$$

Here $C(\alpha,\vec{k})$ is the combination of coefficients which characterizes the phonon spectral peak intensity and $f = \omega/2\pi$ is the phonon frequency. Based on the time history of atomic velocities generated by MD simulations and eigen-displacements from LD calculations, the normal-mode coordinates can be obtained according to Eq. (6). Then, the SED function can be constructed and fitted with Eq. (9) to extract the anharmonic phonon frequency $f(\alpha,\vec{k})$ and lifetime $\tau(\alpha,\vec{k})$.

It should be emphasized that for both the time-domain and frequency-domain NMA, not all of the $\vec{k}$ vectors are allowed in a specific MD domain due to the periodicity requirements. Only those $\vec{k}$ vectors in the first Brillouin zone associated with the chosen unit cell satisfying $e^{-i\vec{k}\cdot\vec{r}} = 1$ can be supported by the MD domain and thus resolved. Here, $\vec{r} = \sum_{i=1}^{3} n_i \mathbf{A}_i$, where $\mathbf{A}_i$ is the length vector of the MD domain in direction i. As a result, thermal conductivity contributions from phonons with very long wavelength, which are near zone center phonons, are excluded. The exclusion of these modes may lead to domain size effects. Nonetheless, a reasonably sized simulation domain should preserve the validness of at least the qualitative description of physical processes.

3 Results and Discussion

3.1 Anharmonic Phonon Dispersion and Phonon Velocity. LD calculations are first performed to produce harmonic phonon dispersion and polarization vectors of atomic motions, through diagonalizing dynamical matrix using GULP. A single rhombohedral primitive cell is computed in GULP and 13 $\vec{k}$ points are sampled between 0 and π/a along the Γ-Z direction. a is the lattice parameter, 10.478 Å for the rhombohedral unit cell. MD simulation is then conducted to compute equilibrium positions and displacements of all of the atoms. At every MD step, normal-mode amplitude S_j is calculated according to Eq. (4), combining information of wave vectors and polarization vectors. The MD simulation domains contain 6, 9, and 12 rhombohedral unit cells along each direction of three primitive vectors, with periodic boundaries conditions. Starting with a pre-equilibrated sample, MD runs in NVE (constant atom number, volume and total energy) ensemble for 400 ps to calculate equilibrium positions of all of the atoms and then another 5 ns to compute normal-mode amplitudes. For every phonon branch, normal-mode amplitudes of each phonon mode will be output at each MD step and stored in a file for post analysis.

Following the method described in Sec. 2.1, the anharmonic phonon dispersion curves at 300 K are constructed through TD-NMA, marked as red dots in Fig. 2(*a*), where 6 out of 15 phonon branches are shown, along the Γ-Z direction. Compared with harmonic phonons calculated with LD, shown as closed dots, anharmonic phonons at 300 K are softened and hence the phonon dispersion curve is flattened due to anharmonicity. Anharmonicity at finite temperatures comes from two aspects: lattice expansion on temperature rise and anharmonic interaction among atoms. To evaluate contribution to anharmonicity solely from lattice expansion around 300 K, a quasi-harmonic case is evaluated, for which LD calculation is conducted in GULP but with the lattice constants

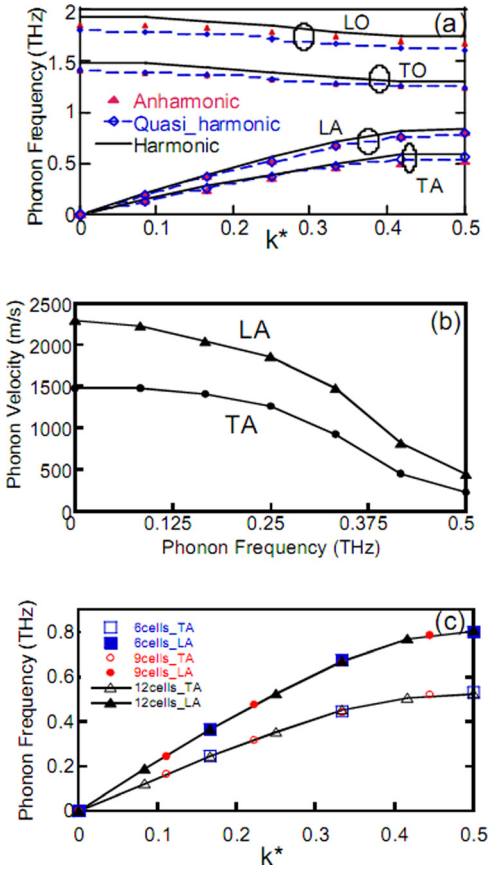

Fig. 2 (*a*) Dispersion curves of longitudinal and transverse acoustic phonons. Solid lines: harmonic LD results (0 K); dashed lines with open diamonds: quasi-harmonic results; solid triangles: anharmonic NMA results (300 K); (*b*) Velocity of longitudinal and transverse acoustic phonons. (*c*) Anharmonic phonon dispersion computed with different sample sizes.

of 300 K. Quasi-harmonic results, shown as blue lines in Fig. 2(*a*), indicate that the anharmonicity at 300 K mainly comes from lattice expansion.

The predicted phonon frequency of the LO phonon at Γ point is about 1.85 THz, agreeing well with the experimental result 1.86 THz [5]. Figure 2(*c*) gives the anharmonic dispersion curves of acoustic phonons computed with different sample sizes, indicating that the size effect is negligible. Phonon velocities are obtained by calculating the slope of phonon dispersion curves. The predicted sound velocity with the TD-NMA is about 2300 m/s for Bi_2Te_3, about 10% smaller than that measured in pump-probe experiments, ~2600 m/s [4].

3.2 Phonon Lifetime. Figure 3(*a*) illustrates lifetimes of acoustic and optical phonons for both longitudinal and transverse polarizations along Γ-Z direction at 300 K, predicted by the TD-NMA. Three regions are marked in Fig. 3(*a*) as acoustic phonons, low-frequency optical phonons, and high-frequency optical phonons. The phonon lifetimes increase when the wave vector becomes smaller (wavelength becomes longer). The optical phonon lifetimes are about the same order as those acoustic phonons near the edge of the Brillouin zone. No obvious size effect other than uncertainty is observed in phonon lifetimes when computing with different sample sizes. It is also noted that the lifetimes of acoustic phonons generally exhibit power law dependence on phonon frequencies as $\tau \propto f^{-2}$, as predicted by Klemens [18]. Figure 3(*b*) plots the fitting for LA phonons, including results from all three simulations domains to obtain sufficient number of

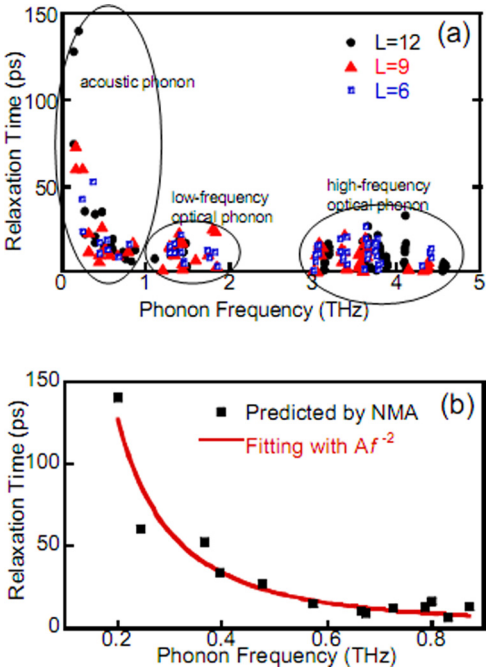

Fig. 3 (*a*) Lifetimes of phonons along the Γ-Z direction computed using TD-NMA, *L* represents the number of cells along *c*-axis. (*b*) Lifetimes of low-frequency acoustic phonons along Γ-Z direction and their power law fittings.

$\vec{k}$ points near the Γ point. The longitudinal acoustic phonons detected in experiments reported previously [4] have a wavelength of about 125 nm, corresponding to a wave vector about 0.05 nm^{-1} and a frequency of 0.016 THz. To access phonons with wavelength as long as 125 nm, a simulation domain larger than 120 unit cells along the *c*-axis (more than 48,600 atoms) is required, which poses computational challenges. Therefore, instead of direct computation, the lifetimes of acoustic phonons with long wavelength/low wave vectors can be extracted from the power law fitting. The lifetimes of the 125 nm-phonon extrapolated from the TD-NMA are 16.9 ns, which is consistent with experimental measurements [4], where the 125 nm phonon does not show obvious decay when traveling for about 400 ps in Bi_2Te_3.

The lifetime of the A_{1g} optical phonon at the Γ point predicted by TD-NMA is 4.2 ps, following the same approach of calculating the lifetimes of acoustic phonons. Alternatively, by using the FD-NMA at the Γ point and fitting the spectral peak of A_{1g} optical phonon mode to Eq. (9), the corresponding lifetime is found to be 5.6 ps. These predicted lifetimes agree with the experimental result (5.3 ps) obtained using ultrafast time-resolved measurements [5].

3.3 Cross-Plane Lattice Thermal Conductivity. A complete set of mode-wise lattice thermal conductivity requires multiple discrete points in the first Brillouin zone, outlined by primary symmetry directions. This would involve a large amount of calculations for Bi_2Te_3 because of its complex Brillouin zone and proper simplifications are sought. Because of the large aspect ratio of in-plane and cross-plane lattice constants, the first Brillouin zone of Bi_2Te_3 has a disk-like shape. If isotropic phonon dispersion in the in-plane radial direction is assumed and with the volume of the first Brillouin zone roughly preserved, the lattice thermal conductivity can be expressed as follows:

$$\kappa_L^z = \frac{1}{2\pi^2}\sum_{\alpha}\int_0^{k_{z,\max}}\int_0^{k_{x,\max}} c_V v_{g,z}^2(k_x,k_z)\tau(k_x,k_z)k_x dk_x dk_z \qquad (10)$$

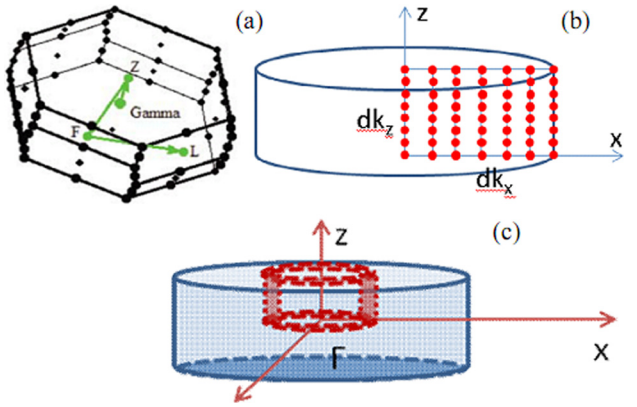

Fig. 4 (*a*) The Brillouin zone of Bi_2Te_3. (*b*) Approximation of the Brillouin zone with a cylindrical disk and the corresponding discretized *k*-grid in the Z-Γ-X plane. (*c*) Integration of the whole cylindrical disk to estimate the total thermal conductivity.

where the double integration of k_x, k_z goes up to the Brillouin zone boundaries $k_{x,\max}$, $k_{z,\max}$ in each direction. Under this approximation, the Brillouin zone is effectively approximated as a cylindrical disk, as shown in Fig. 4(*a*).

The discretized *k*-grid is illustrated in Fig. 4(*b*). Therefore, according to Eq. (10), the thermal conductivity is evaluated as a sum of contributions from rings with radius equals to k_x, thickness equals to Δk_x, and height equals the Brillouin zone thickness in the z direction, as illustrated in Fig. 4(*c*). Due to the finite size of the simulation domain, thermal conductivity contributions from phonons with very long effective wavelength in *x* direction are excluded. The exclusion of these modes will lead to domain size effects in thermal conductivity prediction.

The size effect is tested using three simulation domains $6\times4\times4$, $12\times8\times4$, and $24\times4\times4$ within the FD-NMA. It is also found that the phonon relaxation times are not significantly affected by the different domain sizes, indicating they are well-converged. As suggested by Turney et al. [15] and Schelling et al. [19], the inverse of the thermal conductivity is linearly proportional to the system size. In the present study, due to the use of isotropic approximation, we expect the inverse of thermal conductivity to be linearly proportional to the inverse of the dimension in *x* direction. As seen in Fig. 5, the data do show good linear correlation and the inverse of the *y*-intercept of the linear fitting gives the cross-plane lattice thermal conductivity of bulk Bi_2Te_3. The extrapolated value is 0.85 W/(mK), which does agree well with the value of 0.89 W/(mK) predicted using Green-Kubo's method and the same two-body classical potentials in our earlier work [8]. Using the same approach, the extrapolated lattice thermal conductivity from TD-NMA is 0.93 W/(mK).

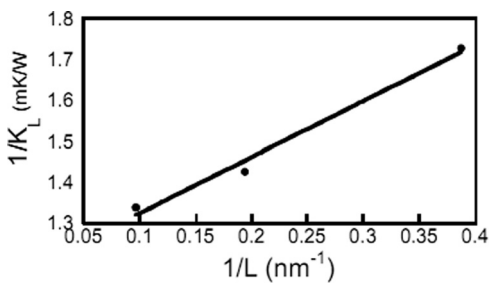

Fig. 5 Inverse of lattice thermal conductivity obtained based on Eq. (10) as a function of the inverse of simulation domain length *L* in *x* direction. The straight line is the linear fit for extrapolation.

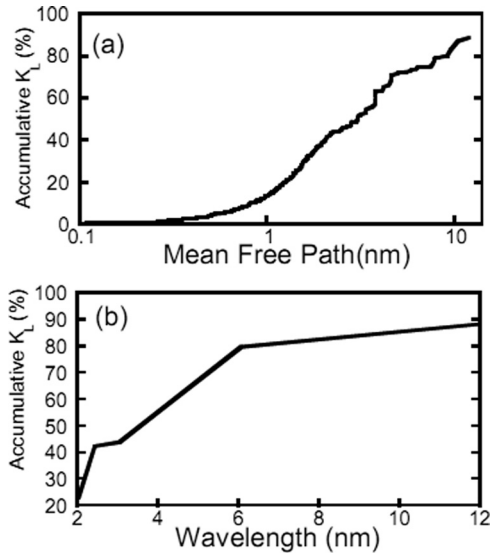

Fig. 6 Percentage of accumulative thermal conductivity (*a*) with respect to phonon mean free path and (*b*) with respect to phonon wavelength

Figure 6(*a*) shows the contributions to the lattice thermal conductivity with respect to phonon mean free path, computed with the $12 \times 12 \times 12$ simulation domain in TD-NMA. Phonons with mean free path between 1 and 10 nm comprise about 80% of the total lattice thermal conductivity. Figure 6(*b*) shows the contributions to lattice thermal conductivity of different phonon wavelengths, indicating that about 80% of the thermal conductivity is attributed to phonons with wavelength less than 6 nm. Due to the limited number of discretized $\vec{k}$ points, the accumulative lattice thermal conductivity in Fig. 6(*b*) does not have the smoothness as that in Ref. [2]. The results shown in Fig. 6 provide new insight to the size dependence of thermal conductivity in nanostructured Bi_2Te_3. In particular, since the maximum phonon mean free path in nanostructures is approximately equal to or less than the characteristic dimension size (thickness for thin film, diameter for nanowires and nanoparticles), Bi_2Te_3 nanostructures with a sub-10 nm characteristic size are needed to achieve significant reduction of lattice thermal conductivity in order for enhanced ZT. For example, Venkatasubramanian [20] has shown the minimum lattice thermal conductivity in Bi_2Te_3/Sb_2Te_3 superlattice with periods between 4 and 6 nm, which are comparable to the wavelengths of these dominant phonons. It should be noted that many early measurements have shown a few times to an order of magnitude reduction in thermal conductivity in 20–100 nm nanostructures, such as in Ref. [21]. In light of our simulation data, those low values are unlikely due to the size effect alone. Instead, point defects, impurities, grain boundaries (in polycrystal nanostructures), and nonuniform composition might be responsible. Therefore, one should be cautious in dealing with nanostructures for the search of ZT enhancement. On the other hand, a recent experimental measurement on a 52-nm Bi_2Te_3 nanowire [22] and an MD simulation on a 30-nm Bi_2Te_3 nanowire [23] both show little reduction in thermal conductivity, which are consistent with our results here.

4 Summary

We adopted time-domain and frequency-domain normal-mode analyses to calculate phonon dispersion relation and phonon relaxation times in bismuth telluride. Phonon velocities were extracted from the gradients of phonon dispersion, which was calculated with TD-NMA. Lifetimes of the A_{1g} optical phonon at the Γ point predicted by TD-NMA and FD-NMA agree with the experimental value, and the lifetimes of acoustic phonons are consistent with the experimental observation of the 125 nm-wavelength longitudinal acoustic phonon. By combining the frequency-dependent anharmonic phonon group velocities and lifetimes, mode-wise thermal conductivities are predicted to reveal the contributions of heat carriers with respect to phonon mean free path and wavelength. It is found that over 80% of the lattice thermal conductivity is contributed by phonons with mean free path below 10 nm, indicating that Bi_2Te_3 nanostructures with sub-10 nm feature size are needed to achieve significant size effect in lattice thermal conductivity.

Acknowledgment

Support to this work by the National Science Foundation and the Air Force Office of Scientific Research is gratefully acknowledged.

Nomenclature

$\mathbf{A}_i$ = length vector of the MD domain in direction i
C_v = mode-wise volumetric heat capacity, $m^2\ kg\ s^{-2}\ K^{-1}$
$C(\alpha, \vec{k})$ = coefficients for the phonon spectral peak intensity, eV/Hz
D_e = depth of potential well, eV
E_j = mode-wise total energy, eV
$\hat{d}$ = atomic displacement from their equilibrium position, Å
f = phonon frequency, THz
$\vec{k}$ = wave vector, m^{-1}
q = effective charge
r_{ij} = interatomic distance, Å
r^0 = equilibrium position of atom, Å
r_c = cut-off distance of Wolf's summation, Å
S = normal-mode amplitude, Å
U = interatomic potential, eV
α = mode polarization (LA, TA, LO, and TO)
Γ = phonon spectral line width, ps^{-1}
σ = bond elasticity of interatomic potential, $Å^{-1}$
$\vec{\varepsilon}$ = polarization vector associated with the direction of motions, unit vector
K_L = total thermal conductivity, W/mK
κ_j = mode-wise thermal conductivity, W/mK
υ_g = phonon velocity, m/s
τ = phonon relaxation time, ps
ψ = spectral energy density, eV/Hz
ω = angular phonon frequency, rad/s

References

[1] Hook, J. R., and Hall, H. E., 1991, *Solid State Physics*, Vol. xxi, Wiley, Chichester; New York, p. 474.
[2] Henry, A. S., and Chen, G., 2008, "Spectral Phonon Transport Properties of Silicon Based on Molecular Dynamics Simulations and Lattice Dynamics," J. Comput. Theor. Nanosci., **5**, pp. 141–152. Available at http://web.mit.edu/nanoengineering/publications/PDFs/Henry_JCompTheoNanoSci_2008.pdf
[3] Huang, Z., Fisher, T. S., and Murthy, J. Y., 2010, "Simulation of Phonon Transmission Through Graphene and Graphene Nanoribbons With a Green's Function Method," J. Appl. Phys., **108**, p. 094319.
[4] Wang, Y., Liebig, C., Xu, X., and Venkatasubramanian, R., 2010, "Acoustic Phonon Scattering in Bi_2Te_3/Sb_2Te_3 Superlattices," Appl. Phys. Lett., **97**, p. 083103.
[5] Wang, Y. G., Xu, X. F., and Venkatasubramanian, R., 2008, "Reduction in Coherent Phonon Lifetime in Bi_2Te_3/Sb_2Te_3 Superlattices," Appl. Phys. Lett., **93**, p. 113114.
[6] Wu, A. Q., Xu, X., and Venkatasubramanian, R., 2008, "Ultrafast Dynamics of Photoexcited Coherent Phonon in Bi_2Te_3 Thin Films," Appl. Phys. Lett., **92**, p. 011108.
[7] Huang, B. L., and Kaviany, M., 2008, "Ab Initio and Molecular Dynamics Predictions for Electron and Phonon Transport in Bismuth Telluride," Phys. Rev. B, **77**, p. 125209.
[8] Qiu, B., and Ruan, X. L., 2009, "Molecular Dynamics Simulations of Lattice Thermal Conductivity of Bismuth Telluride Using Two-Body Interatomic Potentials," Phys. Rev. B, **80**, p. 165203.
[9] Richter, W., Kohler, H., and Becker, C. R., 1977, "Raman and Far-Infrared Investigation of Phonons in Rhombohedral V_2-V_3 Compounds—Bi_2Te_3, Bi_2Se_3, Sb_2Te_3 and $Bi_2(Te_{1-x}Se_x)_3$ $(0 < x < 1)$, $(Bi_{1-y}Sb_y)_2Te_3$ $(0 < y < 1)$," Phys. Status Solidi B, **84**, pp. 619–628.

[10] Wolf, D., Keblinski, P., Phillpot, S. R., and Eggebrecht, J., 1999, "Exact Method for the Simulation of Coulombic Systems by Spherically Truncated, Pairwise r^{-1} Summation," J. Chem. Phys., **110**, pp. 8254–8282.
[11] McGaughey, A. J. H., and Jain, A., 2012, "Nanostructure Thermal Conductivity Prediction by Monte Carlo Sampling of Phonon Free Paths," Appl. Phys. Lett., **100**, p. 061911.
[12] Kaviany, M., 2008, *Heat Transfer Physics*, Vol. xxi, Cambridge University Press, Cambridge, UK, p. 661.
[13] Gale, J. D., 1997, "GULP: A Computer Program for the Symmetry-Adapted Simulation of Solids," J. Chem. Soc., Faraday Trans., **93**, pp. 629–637.
[14] McGaughey, A. J. H., and Kaviany, M., 2004, "Quantitative Validation of the Boltzmann Transport Equation Phonon Thermal Conductivity Model Under the Single-Mode Relaxation Time Approximation," Phys. Rev. B, **69**, p. 094303.
[15] Turney, J., Landry, E., McGaughey, A., and Amon, C., 2009, "Predicting Phonon Properties and Thermal Conductivity From Anharmonic Lattice Dynamics Calculations and Molecular Dynamics Simulations," Phys. Rev. B, **79**, p. 064301.
[16] Ladd, A. J. C., and Moran, B., 1986, "Lattice Thermal Conductivity: A Comparison of Molecular Dynamics and Anharmonic Lattice Dynamics," Phys. Rev. B, **34**, pp. 5058–5064.
[17] Larkin, J. M., Massicotte, A. D., Turney, J. E., McGauphey, A. J. H., and Amon, C. H., "Comparison and Evaluation of Spectral Energy Methods for Predicting Phonon Properties," J. of Comp. and Theoretical Nano. (to be published).
[18] Klemens, P. G., 1951, "The Thermal Conductivity of Dielectric Solids at Low Temperatures—Theoretical," Proc. R. Soc. London, Ser. A, **208**, pp. 108–133.
[19] Schelling, P. K., Phillpot, S. R., and Keblinski, P., 2002, "Comparison of Atomic-Level Simulation Methods for Computing Thermal Conductivity," Phys. Rev. B, **65**, p. 144306.
[20] Venkatasubramanian, R., 2000, "Lattice Thermal Conductivity Reduction and Phonon Localizationlike Behavior in Superlattice Structures," Phys. Rev. B, **61**, pp. 3091–3097.
[21] Borca-Tasciuc, D. A., Chen, G., Prieto, A., Martín-González, M. S., Stacy, A., Sands, T., Ryan, M. A., and Fleurial, J. P., 2004, "Thermal Properties of Electrodeposited Bismuth Telluride Nanowires Embedded in Amorphous Alumina," Appl. Phys. Lett., **85**, pp. 6001–6003.
[22] Mavrokefalos, A., Moore, A. L., Pettes, M. T., Li, S., Wang, W., and Li, X., 2009, "Thermoelectric and Structural Characterizations of Individual Electrodeposited Bismuth Telluride Nanowires," J. Appl. Phys., **105**, p. 104318.
[23] Qiu, B., Sun, L., and Ruan, X. L., 2011, "Lattice Thermal Conductivity Reduction in Bi_2Te_3 Quantum Wires With Smooth and Rough Surfaces: A Molecular Dynamics Study," Phys. Rev. B, **83**, p. 035312.